

GEOLOGY AND PALAEOENVIRONMENT OF KARIN TAK CAVE (LESSER CAUCASUS)

Avagyan Ara^{1*}, Sahakyan Lilit H.¹, Igityan Hayk¹, Gevorgyan Mikayel¹, Sahakyan Kristina¹, Antonosyan Maria², Tepanosyan Gevorg³, Sahakyan Lilit V.³, Atalyan Tatul¹, Grigoryan Taron¹, Aspaturyan Narek⁴, Avagyan Seda¹, and Yepiskoposyan Levon⁵

Abstract

Karin Tak cave is located in the south-eastern end of the Lesser Caucasus (NE of the Armenian Highland). Development of the cave was related to the dissolution of Middle-Upper Jurassic limestone by meteoric water recharge controlled by pre-existing faults and fissures beginning in the Neogene. Geophysical studies of the cave, including by ground penetrating radar, have been conducted, and a map of the pit's walls constructed showing the extent of the roof collapse breccia and of sediment deposits on the cave floor. The collapse material consists of chaotic limestone breccia and blocks. Careful analysis of cave floor sediments allowed the Late Pleistocene palaeoenvironment in the vicinity of the cave to be reconstructed. Analyses included integrated sedimentological studies (stratigraphy, grain size analysis) together with geochemical (X-ray fluorescence) and palynological observations. Pollen studies indicate the dominance of conifers (>60 % *Tsuga sp.*, *Pinus sp.*) together with *Fraxinus sp.* (fam. *Oleaceae*) and *Quercus sp.* (fam. *Fagaceae*), which indicate a cold temperate continental climate in the Late Pleistocene. Non-dramatic climate change occurred during the Last Glacial Maximum (LGM) in the cave area, with conditions favorable for hominin activity.

INTRODUCTION

The Lesser Caucasus is part of the geologically active Alpine-Himalayan orogenic belt and is composed of a variety of different types of magmatic, metamorphic, and sedimentary rocks including remnant oceanic crust. Sedimentary rocks include thick carbonates of Jurassic-Cretaceous age (e.g., Shikhaylibeli et al., 1994) that have been karstified in places as a result of subaerial exposure with the development of karst landforms and cave systems. One such karst cave occurs at Karin Tak in the SE-most Lesser Caucasus (NE Armenian Highland: Fig. 1) where a Late Pleistocene to Holocene sediment infill has been found to contain well-preserved hominin remains and obsidian tools together with faunal and floral remnants (Stafford and Yepiskoposyan, 2015; Antonosyan, et al., 2019). The importance of the cave derives from the fact that it is located on an established migration route used by hominins (e.g., Adler et al., 2014; Fernández-Jalvo et al., 2016). During the Last Glacial Maximum (LGM), corresponding to MIS 2 (Marine Isotope Stage) (26,500–19,000 calibrated years before present (cal. BP) by Clark et al., 2009) led to ecological restructuring, species redistribution and extinctions (Provan and Bennett, 2008) the Great Caucasus served as climatic buffer for southern areas. Additionally, the ameliorating effects of the Black and Caspian Seas favored the Lesser Caucasus as a biogeographical refugium throughout the Pleistocene (e.g., Gabunia et al., 2000; Bar-Yosef et al., 2011; Fernández-Jalvo et al., 2016).

Cave infilling sediments reflect the geomorphological, climatic, and biological setting of the karst systems, and provide a long-term record of past environments and possible human activity. Sediments at depths of about 0.5 m below the present-day Karin Tak cave floor surface contain evidence from obsidian tools bracketed with ¹⁴C-dated animal bones that the site was inhabited by early humans from at least 42,000 years ago (Stafford and Yepiskoposyan, 2015). The Paleolithic occupations are well-documented in Aghitu-3 Cave (around 65 km WSW from Karin Tak cave) occurred between 36 and 32 ka cal BP and between 29 and 24 ka cal BP (Bertacchi et al., 2020).

The environmental and other conditions of the cave are optimal for the preservation of biomolecules, potentially allowing genomic reconstructions to be made of the prehistoric ecosystem of the region. A human tooth found in the Karin Tak cave is dated to ca. 6900 years BP yielded high-quality ancient DNA (aDNA) and indicated genetic continuity of the population inhabiting the Armenian Highlands since at least the Neolithic (Margaryan et al., 2017).

Excellent aDNA preservation allowed successful species identification and has improved Late Pleistocene palaeoenvironmental reconstructions for the region (e.g., Antonosyan et al., 2019; Bertacchi et al. 2020). Genetic screening of the bones has indicated a high faunal diversity between ca. >42,000 and 24,803 cal BP. A total of 27 different taxa, represented by 11 mammalian and three avian families were identified (Antonosyan et al., 2019). The genetically recovered tax-

¹Institute of Geological Sciences, National Academy of Sciences of Republic of Armenia (NAS RA), 24a M. Baghramyan ave., Yerevan 0019, Armenia

²Russian-Armenian University, 123 Hovsep Emin St, Yerevan 0033, Armenia

³Center for Ecological-Noosphere Studies, NAS RA, 68 Abovyan St., Yerevan 0025, Armenia

⁴Yerevan State University, 1 Manukyan St., Yerevan, 0025, Armenia,

⁵Institute of Molecular Biology, NAS RA, 7 Hasratyan St., Yerevan 0014, Armenia

* Corresponding author: avagn1064@gmail.com

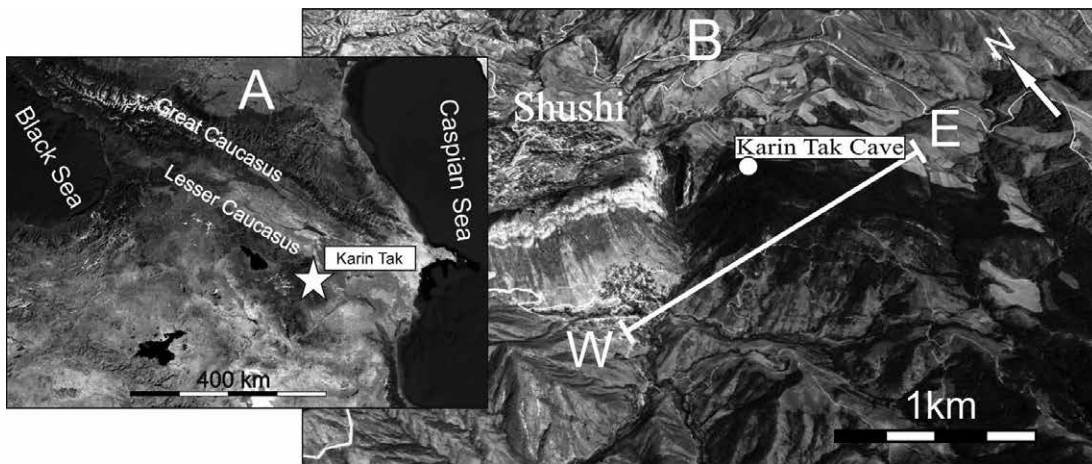


Figure 1. (A) Geographic location of Karin Tak Cave in the Lesser Caucasus (SE part of Armenian Highland), (B) Situation of Karin Tak cave on the Google Satellite 3D Image. SW-NE cross section for schematic model of cave development (Figure 14).

onomic composition rich and diverse and consists predominantly of extant wild mammalian and avian taxa, together with species that are regionally extinct (including *Gazella subgutturosa*, *Ursus tibetanus*, *Crocota crocuta* and *Mesocricetus raddei*). Overall, the results of the fossil taxonomy indicate the continuity of the faunal composition of the region throughout the Late Pleistocene. It seems, therefore, that the cold and arid conditions during MIS 2 did not cause a change in faunal

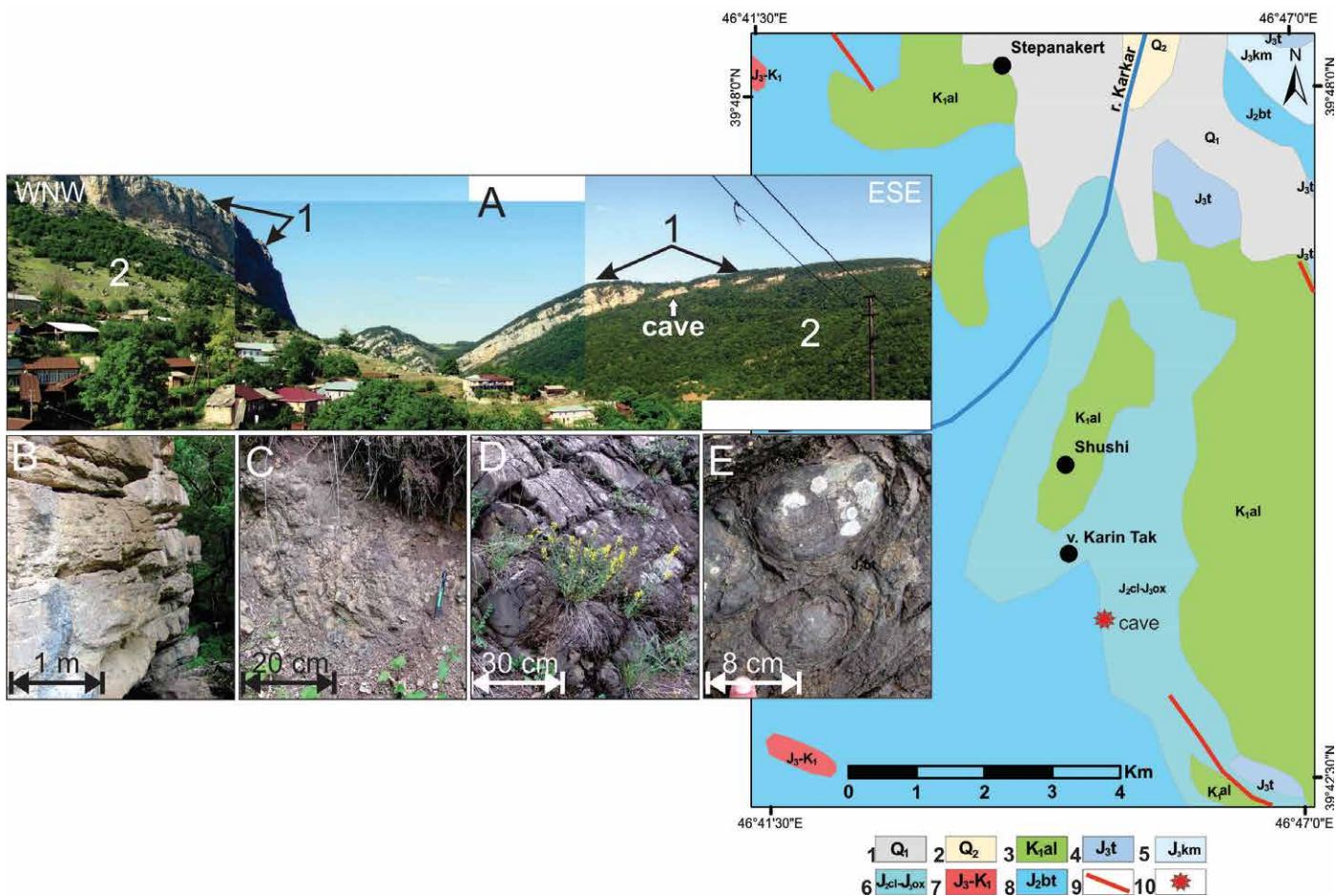


Figure 2. (A) Field photography of Karin Tak cave, (B) Middle and Upper Jurassic (Callovian-Oxfordian) thickly bedded limestones, (C-E) Middle Jurassic, Bathonian sedimentary rocks, (C) volcanic breccias, (D) siltstones, (E) volcanic formations of on-ion-skin weathering. Simplified geological map of the area. 1. Modern sediments, 2. Lower Quaternary sediments, 3. Lower Cretaceous (Albian) pyroclastic rocks, 4. Upper Jurassic (Tithonian) limestones, 5. Upper Jurassic (Kimmeridgian) organogenic-detrital, pelitomorphic, sandy limestones with volcano-sedimentary lenses of small thicknesses, 6. Middle Jurassic (Callovian), Upper Jurassic (Oxfordian) limestones, 7. Upper Jurassic-Lower Cretaceous quartz-diorites, 8. Middle Jurassic volcanic, pyroclastic, volcanosedimentary rocks, 9. Faults, 10. The locality of Karin Tak cave

composition. During that time span, Karin Tak cave was located at the boundary between arid subtropical and humid climate regions (with the latter supporting forests), a pattern similar to the present-day setting of the site (Antonosyan et al., 2019).

The previous results also indicate that Karin Tak cave should be considered as a regionally important site from which viable molecular data can be obtained. These data will allow the reconstruction of the Late Pleistocene ecosystem in the Lesser Caucasus, and will give new insights into the early human occupation and biodiversity of the region.

The principal aims of this paper are therefore to: (i) describe the formation of Karin Tak cave in terms of geological processes; (ii) report on the depth and spatial dimensions of soft sediments in the cave on the basis of geophysical surveys to determine strategies for future excavation; and (iii) present the results of sedimentological, X-ray diffraction, geochemical, and palynological studies of the cave floor sediments to investigate depositional processes and to reconstruct the paleoenvironmental record of the site.

Geological setting of the cave

Karin Tak cave (39°44'35.23" N, 46°45'58.47" E, 1405 masl) is located on the East bank of the Karkar river and is named after a nearby village (Figs. 1, 2). The cave is about 60 m long containing at least six chambers, and is in general oriented NE-SW (Fig. 3). The cave has formed in thickly-bedded Callovian to Oxfordian (Middle-Upper Jurassic) limestones (Shikhaylibeli et al., 1994) that outcrop in the area (Fig. 2, A–B). These limestones typically display grainstone (occasionally packstone) texture and in some places silicification is evident. The bedrock strata dip approximately 18° towards NE near the cave.

The limestones unconformably overlie the Middle Jurassic (Bathonian) volcanoclastic (Fig. 2, C–D), sedimentary and volcanic rocks. The outcropping porphyric basalts display onion skin weathering in places (Fig. 2, E). The Bathonian rocks have a strike of N138°–N142° and dip between 29°–51° NE, which is markedly steeper than the overlying limestones.

In terms of the regional geological structure, the SE Lesser Caucasus is located in an area that underwent intense compression and uplift during the Neogene as a result of convergence between the Arabian Plate and the South Armenian block or microplate (e.g., Avagyan et al., 2010; Sosson et al., 2010). The regression of the Sarmatian sea occurred and continental conditions were initiated in the late Messinian in the Ararat depression to the south of the Lesser Caucasus as a result of Late Miocene tectonic activity and uplift (Gabrielyan et al., 1981; Avagyan et al., 2018).

Middle-Upper Jurassic limestones were probably exposed subaerially at this time and have subsequently undergone karstification. Near-surface caves developed along pre-existing fractures and faults due to meteoric dissolution of the host rock. We suggest that the development of the Karin Tak was initiated during this period.

MATERIALS AND METHODS

Karin Tak cave was studied using conventional geological and structural mapping techniques. Two- and three-dimensional ground penetrating radar surveys were conducted in the cave. An SIR-3000 (USA, 2008) GPR system with a 400 MHz antenna was used, enabling a survey to be made to depths of up to 3 m.

Pit excavations were used to investigate the cave floor sediments. Six sediment layers were identified in the SE and SW walls of the excavated pit in the cave. Sediments were categorized by particle size, texture, and fabric using White's

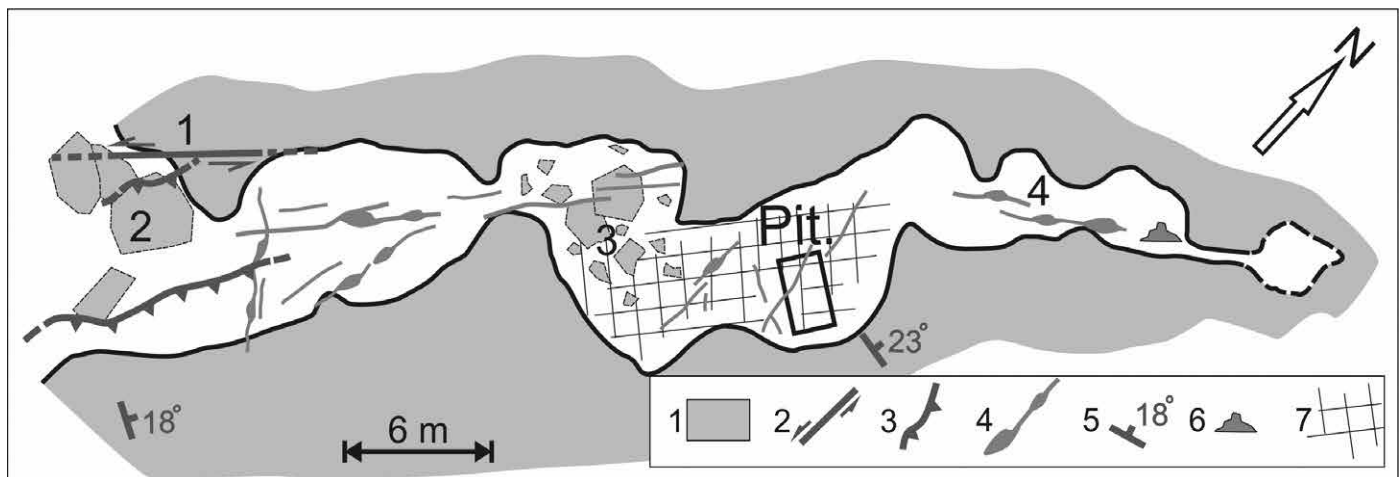


Figure 3. The plan of Karin Tak cave with observed structures. The location of the pit is indicated. 1. Limestones; 2. Strike-slip fault; 3. Reverse faults; 4. Fractures and vertical shafts; 5. Limestone dip; 6. Stalagmites; 7. Profile lines of the geophysical survey.

classification (White, 2007). The Munsell color chart system (<https://munsell.com/>) has been used to define the colors of cave sediments.

The immersion method was used to study the mineralogical content of samples from A–D layers. One hundred grams of sample from each layer were separated into light and heavy fractions by Bromoform liquid. The minerals were studied using liquids of N 1,490 (for light fraction) and 1,530 (for heavy fraction) refractive indexes. For pollen analysis, 10 mL of each dry sediment sample was processed following the method of Grichuk and Zaklinskaya (1948) with the following steps: first adding 20 mL 10 % HCl to each sample with 10 minutes in a hot water bath. Second is adding 20 mL 10 % KOH, 20 minutes in the hot water bath, and the last step is heavy liquid flotation, which contains KJ and CDJ₂. Each step is followed by flushing with distilled water, centrifuging 12 minutes at 3000 rpm in a swing rotor centrifuge and carefully decanting the liquid.

Eleven samples were studied using a conventional light microscope. Nine samples were collected from the cave pit for spectrometry analysis, together with one chert sample. The samples were air-dried, homogenized, sieved (<2 mm), milled in compliance with ISO-11464 (ISO, 2006) and then stored in sealed bags. The cave sediment samples were analyzed by X-ray fluorescence spectrometry using an Olympus Innov-X-5000 (USA) apparatus following EPA standard 6200 (US EPA, 2007) in the Center for Ecological-Noosphere Studies (CENS, Armenia). The XRF was equipped with a Ta X-ray tube that allowed the determination of elements (Cr, V, Ti, Mo, Zr, Sr, Rb, As, Zn, Cu, Co, Fe, Mn, Pb and Ba) in 3-beam soil mode. Beam time was 120 seconds. Detailed quality assurance and quality control (QA/QC) was carried out using standard reference materials (National Institute of Standards and Technology 2711a and NIST 2710a, USA), a blank (SiO₂) obtained from the NIST(USA), as well as lab duplicates. QA/QC showed that the accuracy and precision of the analyses were 2.2–15.4 % and 0.1–6.9 %, respectively. Values below detection limits (BDL) were observed for Mo. Considering the relatively low number of BDL records (<15 % of all samples) (Johnson et al., 2011; Rothwell, and Croudace 2015) element concentrations BDL are given a value of one-half of the detection limit.

RESULTS

Structural features

The general orientation of Karin Tak cave (N 46°) is controlled by the dominant system of regional fractures which trend N 40°–N 55° (Fig. 3). The presence of sinkholes on the surface of the surrounding limestone plateau and of numerous well-developed vertical shafts in the cave indicate intense circulation of meteoric groundwater with the leeching and dissolution of the limestone host rock. Most of the shafts in the cave have developed along fractures and are oval

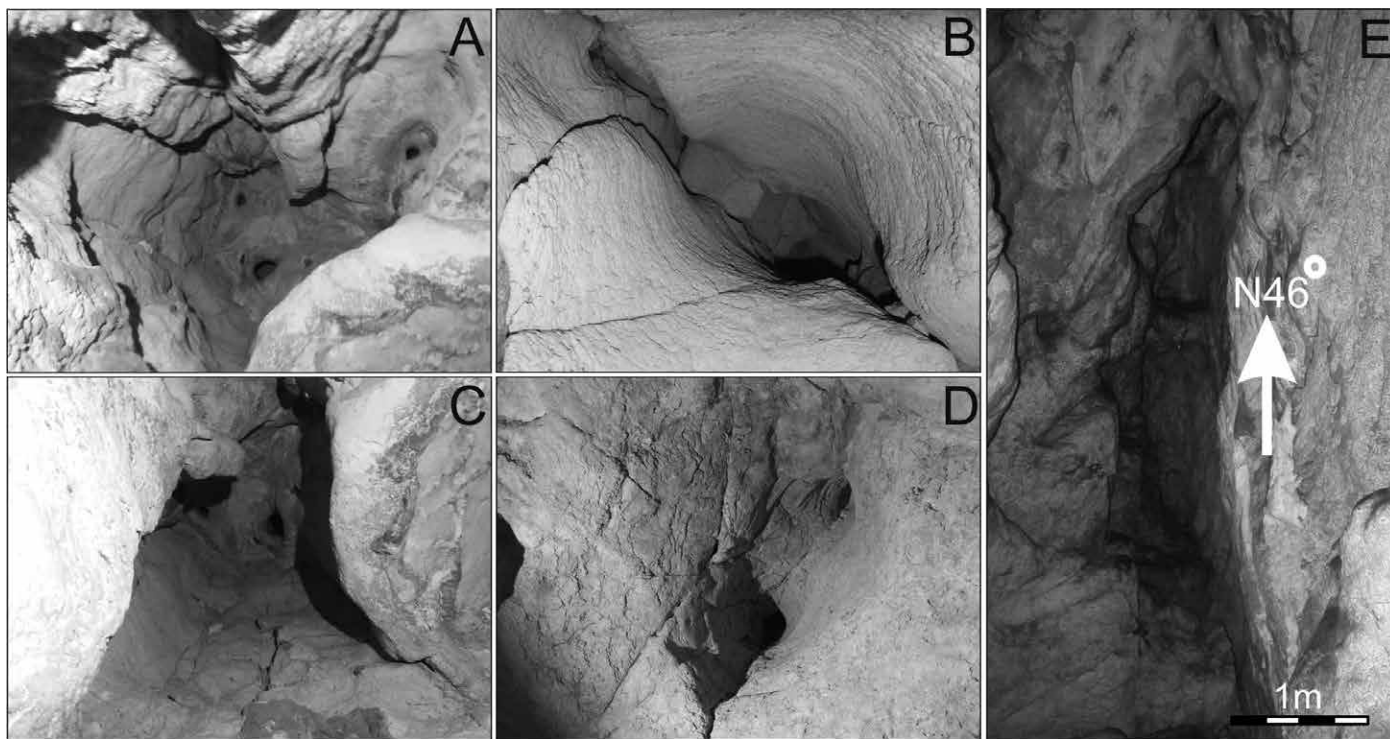


Figure 4. The vertical shafts (A–D) with upward continuation. Most of them routed on the fracture and developed oval-shape sections, (E) The roof of the inner part of the cave showing its development along a pre-existing crack. The location of the roof is shown in Figure 3, marked 4.

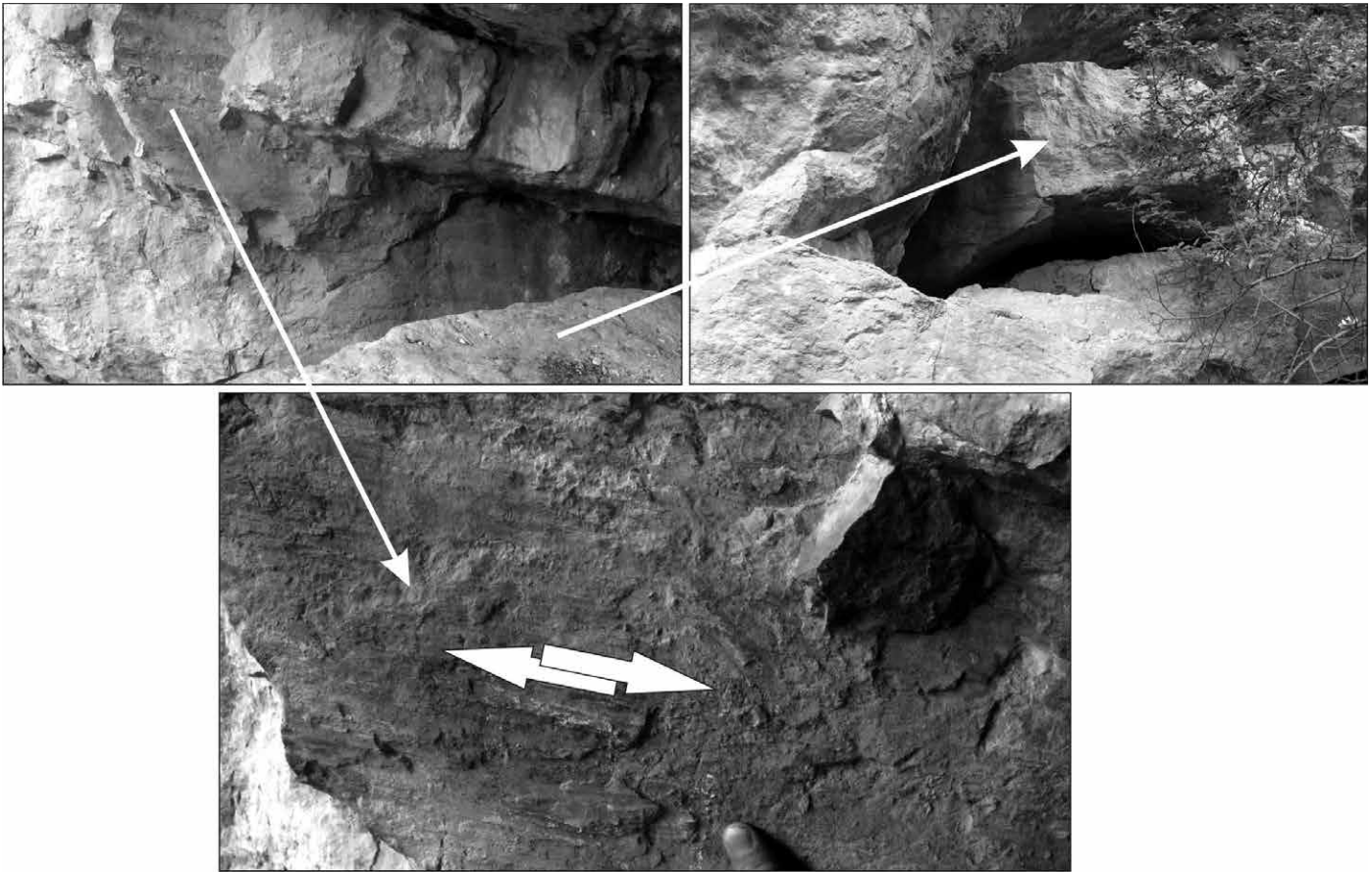


Figure 5. Strike-slip fault near the actual entrance of the cave. Its situation is marked 1 in Figure 3.

in cross-section (Fig. 4). The roof of the inner part of the cave (see area 4 on the cave map in Fig. 3) shows shaft development along a pre-existing fissure (Fig. 4).

Horizontal or oblique-slip movement may have occurred on some of the fractures because a left-lateral strike-slip fault with almost the same strike ($N 50^\circ$) is observed in the northern part of the cave entrance ($N 50^\circ 80^\circ SSE 11^\circ NE$) (see area 1 on the cave map in Fig. 3 and Fig. 5). Reactivation of faults and the opening of subsurface migration routes for meteoric waters had an important role in development of the cave. A number of reverse faults have also been observed near the cave entrance, but do not appear to have had a significant effect on the cave.

Geophysical survey

The ground-penetrating radar allowed qualitative and quantitative surveys of the cave floor deposits. The aerial extent of the geophysical survey in the central chamber is presented by the profile lines in Fig. 3.

The deposits were divided into horizontal layers 0.25 m thick. Horizontal cross-sections of the floor stratum in the chambers with the pit are presented in Figure 6. Layer 1 corresponds to the cave floor surface. The next layer, 0.25 m deep, contains features whose colors were substantially different from those of the background (white color marks limestone blocks and boulders). With increasing depth, contours bounding the buried limestone blocks and the depths of their spreading in the horizontal sections become more apparent (Fig. 6).

Based on data produced by the analysis of two-dimensional GPR surveys, a three-dimensional model was produced (Fig. 7), where the white and green colors correspond to hard limestone blocks; and the dashed lines mark the borders of soft sedimentary deposits. A sedimentary layer is outlined in the central part of the section, and limestone blocks are recorded in more marginal areas.

The GPR surveys reveal the presence of buried limestone blocks and boulders, which are the possible result of cave roof collapse. This suggestion is further verified by ground-truthing in the pit sections through the cave sediment. The location of the pit was chosen according to GPR survey as a place with fewer blocks and boulders.

Sediment sources (collapse and clastic deposits)

Sedimentological investigations of the southeast and southwest walls of the pit (Fig. 3), which was excavated in 2016-2018, showed six stratigraphic layers (Figs 8 and 9).

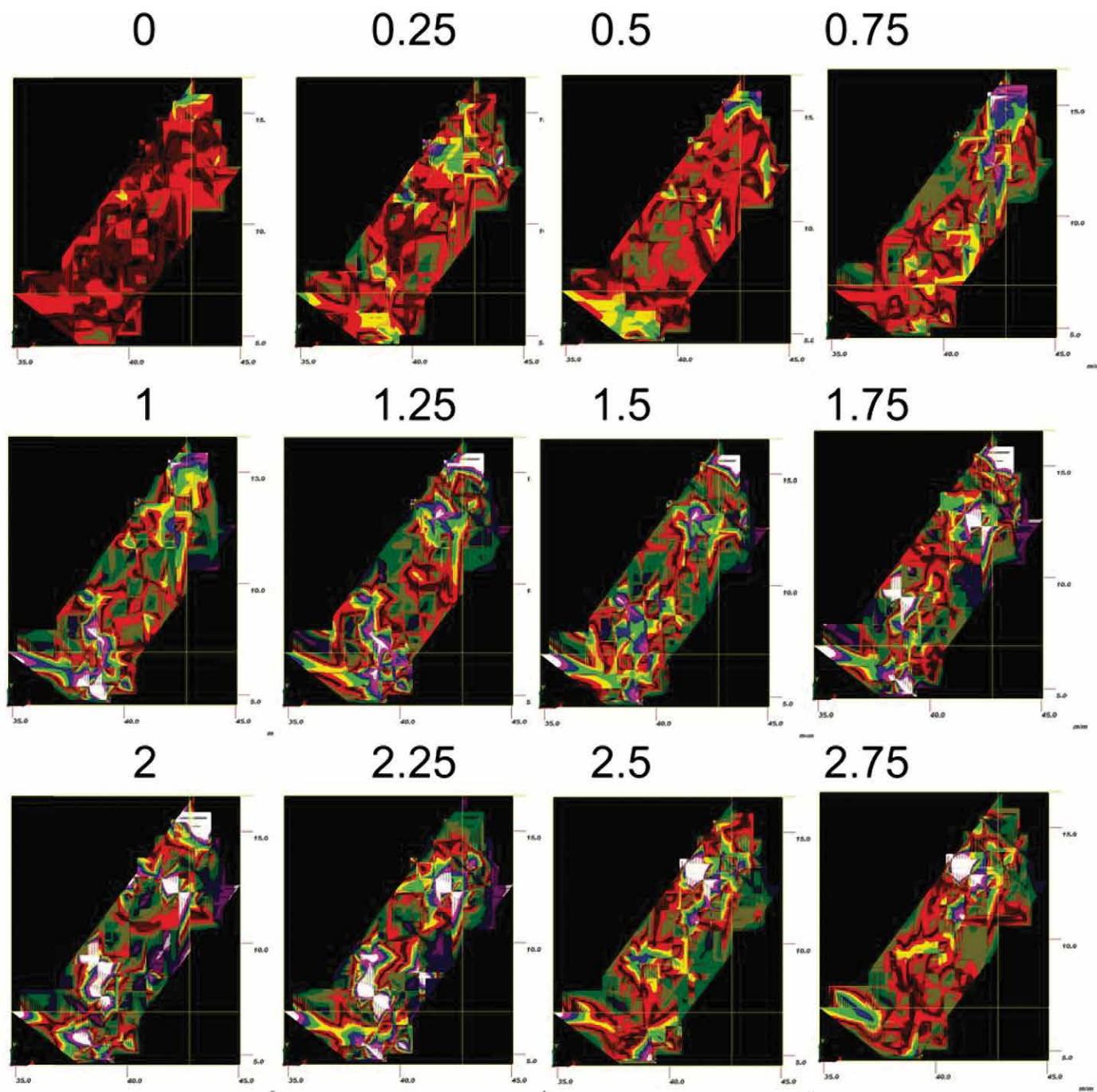


Figure 6. Horizontal sections of the GPR survey along depth (with the step of 0.25 m) in the chambers of the excavated pit (Figure 3) (white color marks buried limestone blocks).

The lowermost layer H (15–40 cm thick) comprises of a strongly calcareous, pale yellow (2.5Y 7/4) silt loam. The observed layers are not, or only slightly, stratified and developed over different time intervals. The coarse collapse debris by contrast developed instantaneously. Layer H has loess-like features and is archeologically barren, containing less material than the overlying layers. Layer H is overlain by layer F (a dark brown (10YR 3/3) sandy loam, up to 30 cm thick) rich in organic matter and demonstrate some post-depositional perturbations (Fig. 9). Layer G presented only in southwest wall of the pit comprises of olive (5Y 5/3) loam with isolated clasts of limestones (0.5–30 cm). Layer E mainly consists of grayish-brown (2.5Y 5/2) calcareous loamy sand (10–70 cm); it contains pale brown clay lens in its upper part (E') and dark grayish-brown (2.5 Y 4/2) lens E''. The latter is composed of calcareous silt containing phytolith particles. Layer D (20–30 cm) is a pale brown (10YR 6/3), silty clay loam displaying a weak stratification. Layer C (5–35 cm) is composed of whitish-grey (2.5Y 7/3), strongly calcareous silty clay-loam with limestone granules and bones. Layer B,

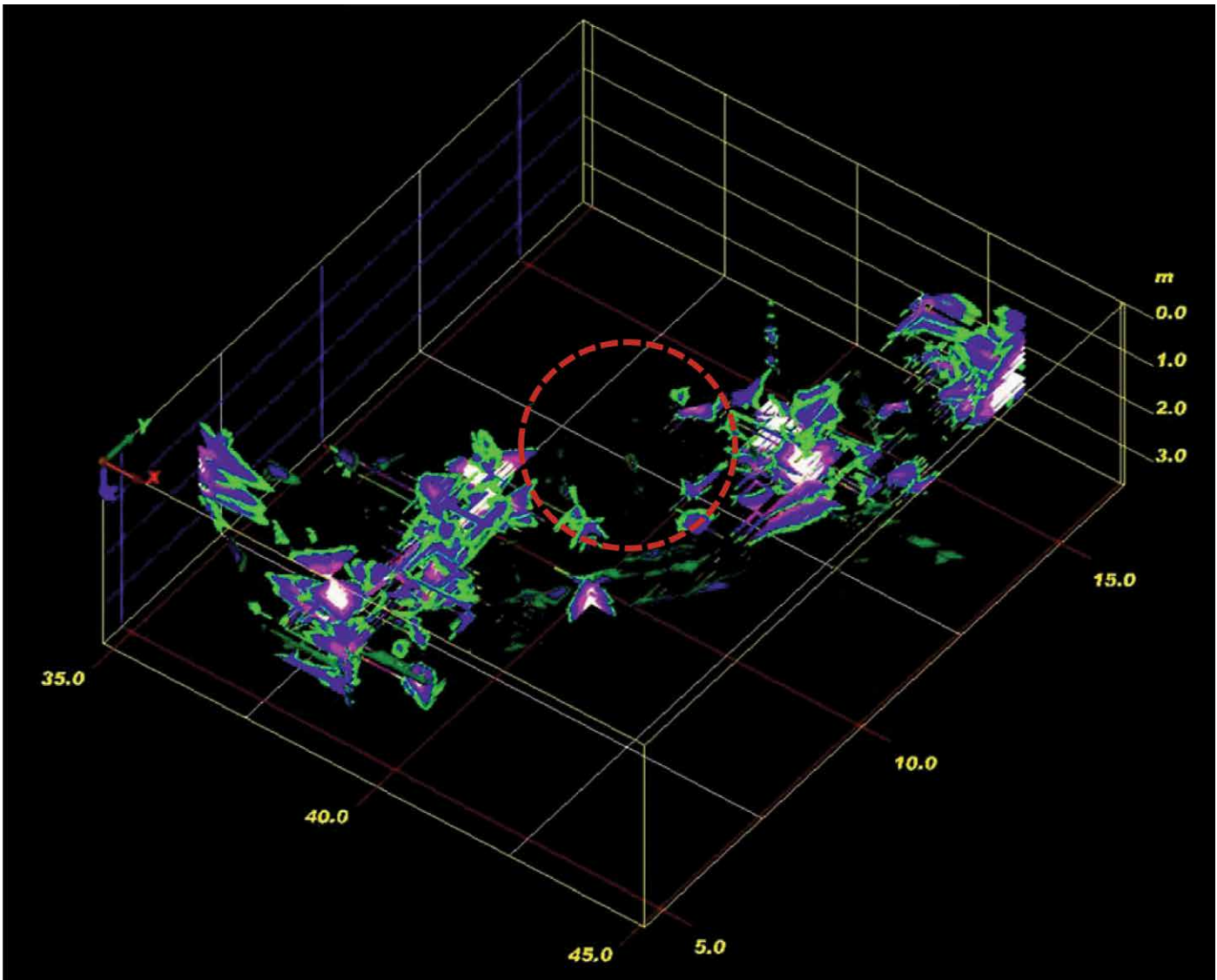


Figure 7. The 3D model of the hall with the pit (the white and gray colors correspond to limestone blocks; the dashed lines encompass the soft sediments).

50–80 cm thick, is a light olive-brown (2.5Y 5/4), friable, calcareous sandy loam and contains small carbonate pebbles.

The layers A and B were formed between $24,589 \pm 149$ BP and $22,947 \pm 204$ BP according to ^{14}C dating on bones from different depths (Antonosyan et al., 2019). The top 2 cm below the present-day cave floor is a blackish calcareous cave sediment horizon (A') which overlies pale-brown (10YR 6/3) loam (5–12 cm) containing pebbles and bones (A).

Karin Tak cave contains a variety of siliciclastic and chemical sediments deposited by a range of mechanisms. Autochthonous deposits are derived from the surrounding bedrock and include collapse breccia and their breakdown products.

Breakdown products consist of fragments of bedrock with a range of clast sizes, most of which result from cave collapse due to seismic activity. Less pronounced collapse features include wedge-shaped debris cones that are developed below collapsed sinkholes (see area 3 on the cave map in Fig. 3). Within the pit excavated in the cave floor, limestone clasts <0.25 m in diameter were observed in the SW wall in layer D (Fig. 9).

Large blocks of limestone were observed near the cave entrance (2 in Fig. 3), which has retreated due to past episodes of collapse. These blocks probably correspond to collapse debris (including limestone blocks and boulders of >0.5 m in diameter) identified by the radar survey and observed in deeper parts of the floor pit (Figs. 7, 8 and 9).

The allochthonous sediments, derived from external sources, include washed-in soils, debris flows, and materials derived from biological (animal and possibly human) activity. The most accentuated layers with these sediments are the layers A, B, C, D, E, and especially F. Detrital sediments include sands and silts deposited from subsurface streams and storm run-off into sinkholes. They are present in practically all layers. Chemical deposits include calcite and gypsum



Figure 8. Photography of the southwest and southeast walls of the excavated pit.

together with oxides and hydroxides of iron and manganese. Speleothems, including stalactites, stalagmites, and stalagnates (columns) are less developed in the biggest chambers and more prominent in the NE end of the cave.

The light mineral composition in sediments from A to D layers is presented mostly by undetermined weathered minerals, lesser amounts of volcanic glass, plagioclase, quartz, phylolith, and opal. The heavy mineral assemblages are characterized by clear predominance of opaque minerals with abundant ilmenite, with lesser amounts of hornblende and diopside. Carbonate content varies from 26.1–38.5 %.

Samples for pollen analyses were taken from the SE and SW walls of the cave-floor pit (Figs 8 and 9). More than 400 grains were counted for each sample, and grain proportions were calculated based on the sum of all palynomorphs present. The results (Fig. 10) point to the presence of abundant organic material in layers A, B and E'. In lens E' and in layer H, no pollen or other palynomorphs were found (Fig. 10).

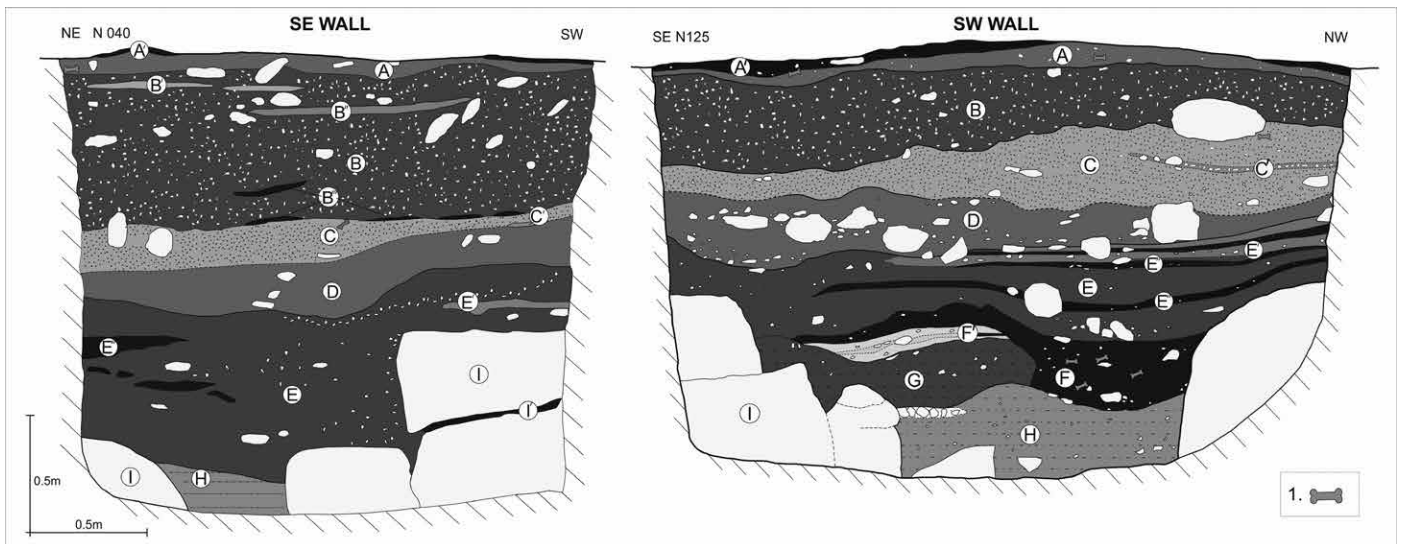


Figure 9. Log of the southwest and southeast walls of the pit. Cave sediment colors according to the Munsell color chart. (A) Pale brown loam with pebbles and bones; (A') Blackish soil horizon; (B) Light olive brown sandy loams with limestone rubbles; (B') Carbonate crust lenses; (B'') Very pale brown strongly calcareous clay lens; (B''') Very dark grayish brown clayey lenses; (C) Light brownish silty clay loam with limestone pebbles, bones; (C') Rubified lens; (D) Pale brown silty clay loam; (E) Grayish brown loamy sand; (E') Pale brown clay lens; (E'') Dark grayish brown calcareous silty lens; (I) Limestone boulders; (I') Very dark grayish clay; (G) Olive loam; (F) Dark brown sandy loam; (H) Pale yellowish brown silt loam; (1) Bones.

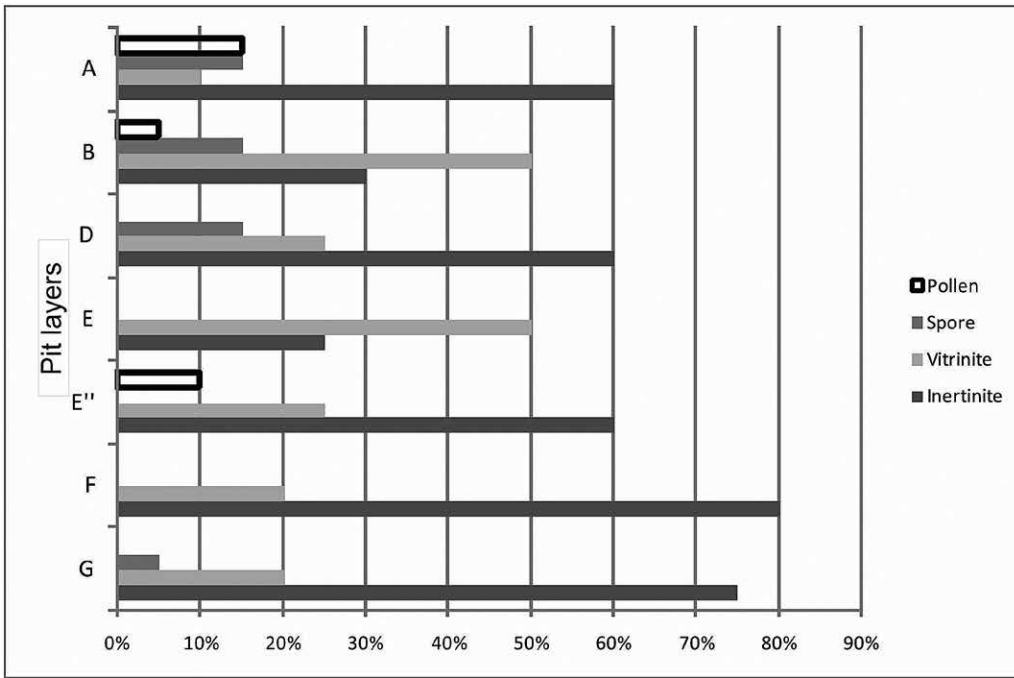


Figure 10. Summary diagram showing pollen and palynomorphs (pollen, spore, vitrinite, inertinite).

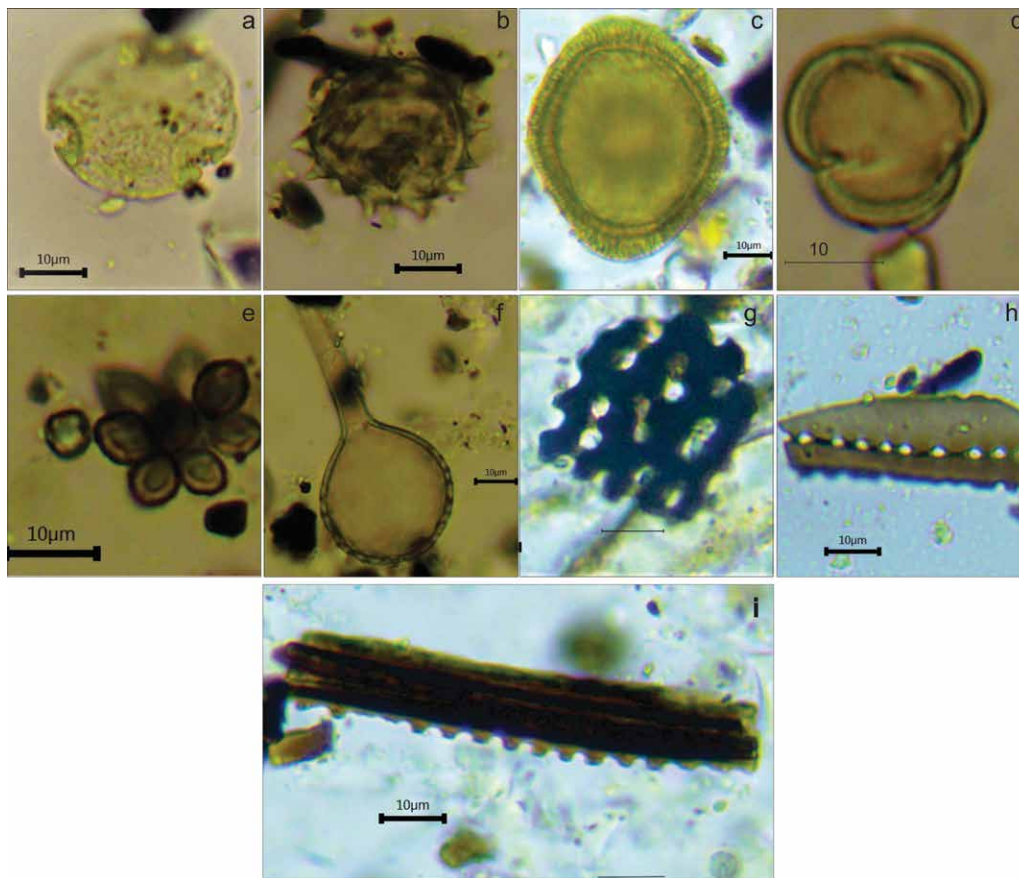


Figure 11. Representative micrographs of pollen and palynomorphs under light microscope: (a) *Tilia* sp. (fam. *Malvaceae*), (b) *Asteraceae* sp., (c) *Tsuga* sp. (fam. *Pinaceae*), (d) *Fraxinus* sp. (fam. *Oleaceae*), (e, f) Fungi, (h, i) Phytoclasts (a, b, f) from the layer (A), (c) (layer B), (d, i) (layer E), (e, g) (layer D), (h, i) (layer F).

A geochemical study of the chert lens observed a few hundred meters from the cave in the upper part of the volcanoclastic rocks showed that some elemental ratios are similar to those in layer F (Fig. 13). Chert, a high-silica rock dom-

Layer A contains pollen from *Tilia* sp. (fam. *Malvaceae*), *Fraxinus* sp. (fam. *Oleaceae*), *Apiaceae* sp., *Asteraceae* sp., *Quercus* sp. (fam. *Fagaceae*), and *Chenopodiaceae* sp. (Fig. 11), layer B contains pollen from *Tsuga* sp. and small amounts of *Pinus* sp. (fam. *Pinaceae*), *Rosaceae* sp., *Quercus* sp. (fam. *Fagaceae*), and *Asteraceae* sp. (Fig. 11). In the lens E'', *Asteraceae* sp. and *Quercus* sp. (fam. *Fagaceae*) pollen were recorded (Fig. 11 a-d). Large amounts of fungal spores, phytoliths, and charcoals were recorded in many samples (Fig. 11 e-i). Pollen preservation was poor and taxonomic resolution to species level was impossible.

Bulk sediment geochemistry: X-ray fluorescence

Nine cave sediment samples from the pit in the floor of Karin Tak cave were analyzed for their contents of elemental Pb, Cr, Pb, Ba, Mo, Cu, Sr, Co, Ti, As, Zn, Zr, V, and Mn (Fig. 12).

Geochemical markers in layers G and F at nearly the same stratigraphic level in the floor pit (SW wall, Fig. 9) show quite different content of Pb, Cr, Rb, Ba, Fe, Co, Ti, As, Zr and V (Fig. 12). Results showed comparable high contents of Pb, Cr, Rb, Ba, Fe, Mo, Co, Ti, As, Zn, Zr, V, and Mn in layer F and depleted contents of Pb, Cr, Rb, Ba, Fe, Co, Ti, As, Zr, and V in layer G. The difference in Mo, Mn and Zn contents are less marked in layers F and G. The layers E, F and G are characterized by peaks in the contents of Cu, Zn, and Mo; Mo enrichment also occurs in layer A.

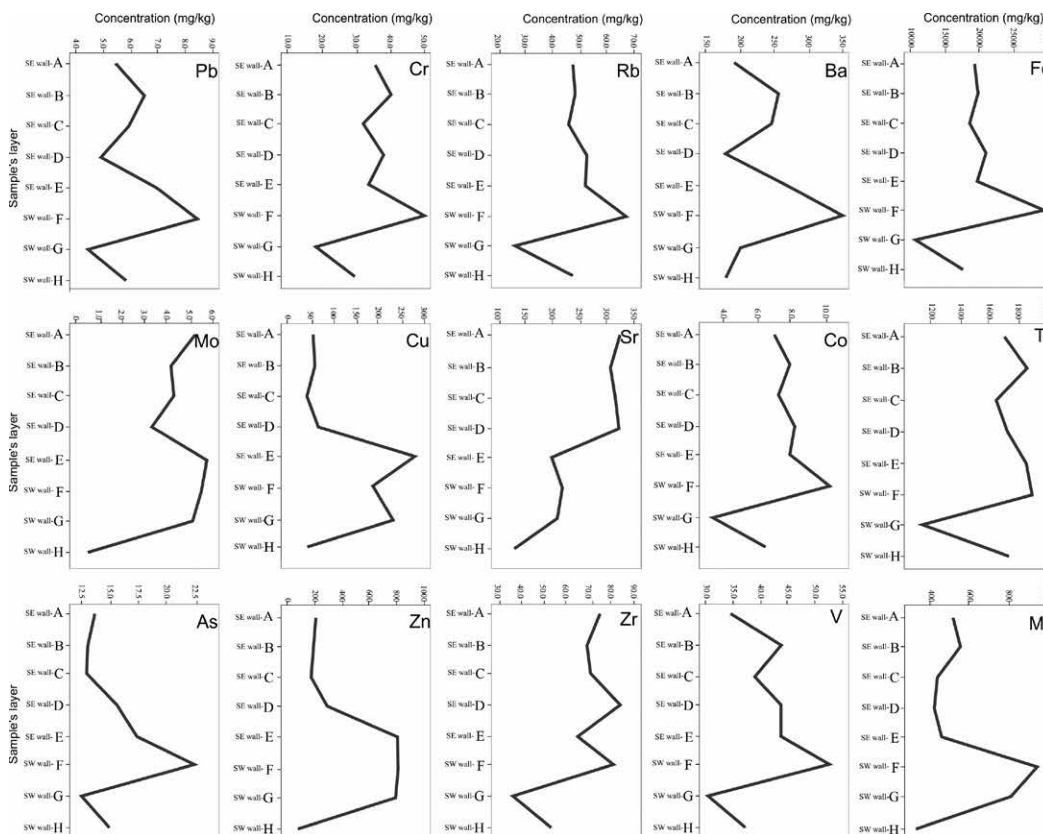


Figure 12. Trace element analyses of the pit layers (A–H).

ical, and climatic factors. The cave originated with Neogene regional uplift when the regression of the Sarmatian Sea occurred and continental conditions were initiated conducive to the exposure of the Jurassic carbonate rocks to the surface and to subaerial weathering and karstification. The cave is developed along NW–SE trending oblique slip faults and fissures indicating a structural control. The presence of numerous vertical shafts in the cave, together with sinkholes and speleothems, indicate its epigenetic nature. Nevertheless, we have observed one or two cupolas, the origin of which

inantly composed of SiO₂ minerals were among the first raw materials utilized by hominine.

In general, the Sr and Zr contents decrease with depth (Fig. 12), as does the content of Mo except for layers E, F and G. The content of V was correlated with that of Ba. Ba shows a positive value in layer F and a negative value in layers A, D, G and H. The loess-like sample from layer H is free of organic material and shows negative anomalies of Mn, Ba, Sr, Zn and Mo.

DISCUSSION

Both external and internal factors control the development of caves in carbonate rocks, and the origin and development of Karin Tak cave was influenced by tectonic, lithological, and climatic factors. The cave originated with Neogene regional uplift when the regression of the Sarmatian Sea occurred and continental conditions were initiated conducive to the exposure of the Jurassic carbonate rocks to the surface and to subaerial weathering and karstification. The cave is developed along NW–SE trending oblique slip faults and fissures indicating a structural control. The presence of numerous vertical shafts in the cave, together with sinkholes and speleothems, indicate its epigenetic nature. Nevertheless, we have observed one or two cupolas, the origin of which is unclear, therefore, in the initial stages, the hypogenic influence is not excluded as in the case of Azokh Cave in the same geographic region, developed in Jurassic limestones (Domínguez-Alonso et al., 2016). Even if there were hypogenic parts in the formation of the cave, it is minimal and epigenetic ones are dominant. Cave development activity is not the same now as it was at the beginning of its formation: after the roof collapse and breakdown no speleothems were formed in the two largest chambers of the cave.

Geophysical investigations in the central cham-

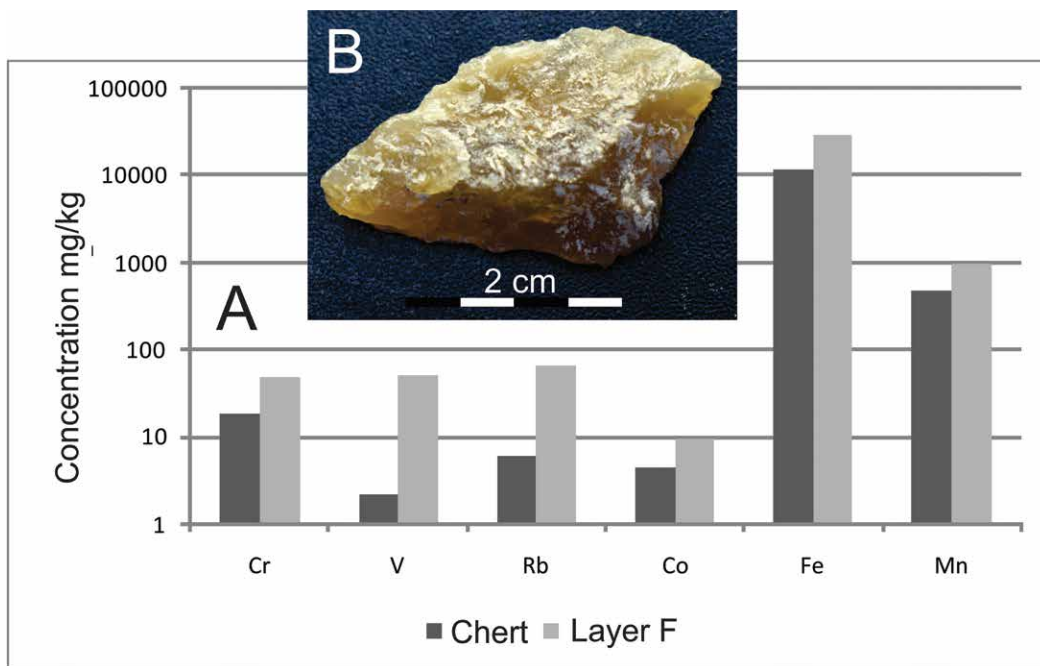


Figure 13. Trace element analyses of the chert and pit layer (F).

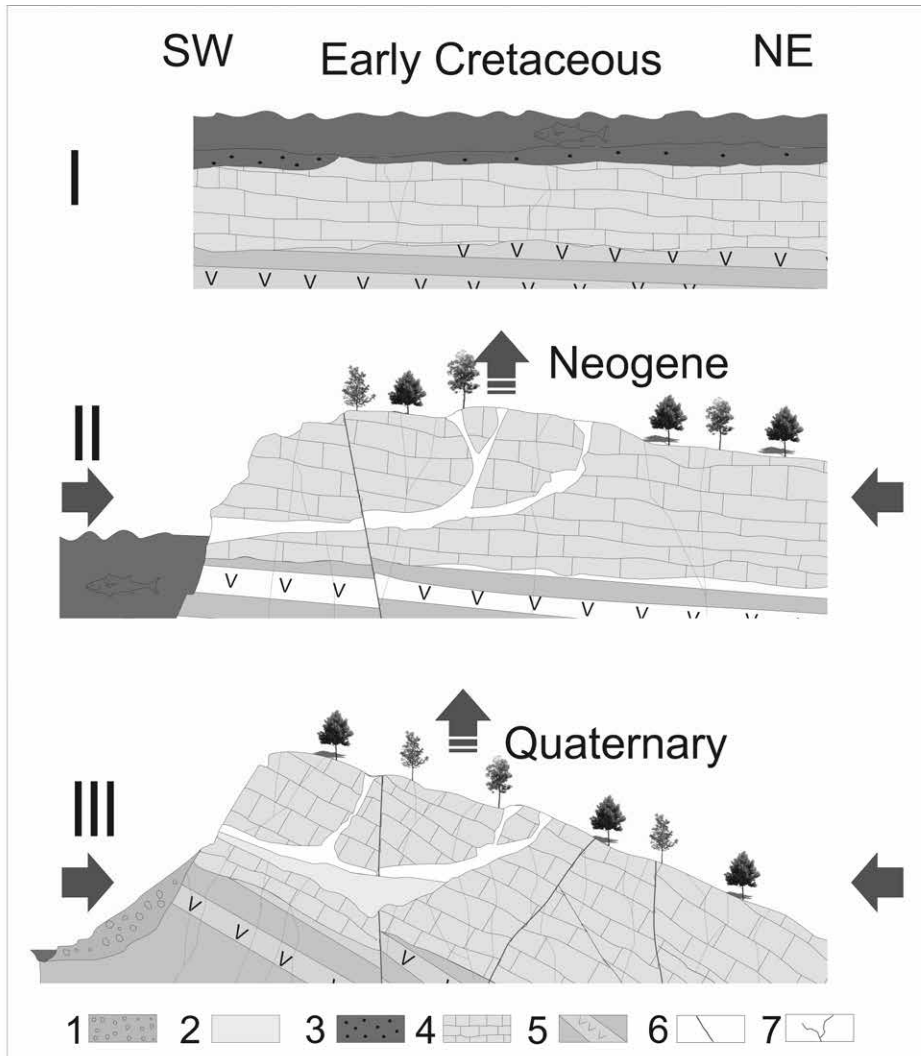


Figure 14. Cave development stages. (I) Cretaceous, (II) Miocene-Pliocene, (III) Pleistocene-Holocene. (1) colluvion, (2) recent cave sediments, (3) dip non-consolidated sediments, (4) Callovian-Oxfordian limestones, (5) Bathonian volcanoclastics, (6) faults, (7) fractures. SW-NE cross section line shown in Figure 1.

dramatic climate change during LGM MIS 2.

The X-ray fluorescence studies of cave sediment samples identified variations in elemental compositions, although the effects of post-depositional contamination (e.g., due to human activity should be carefully considered).

From a stratigraphic point of view, it is interesting to compare the geochemical markers in layers G and F. Although these layers are adjacent (Fig. 9) they show quite different contents. As, Cr, Cu, Pb, Zn, and Ba positive anomalies can be result of concentrations of skeletal and organic detritus or charcoals (e.g., Basta et al., 2005; Calvert and Pedersen, 2007), which are visible by *in situ* observation of layer F.

The increased concentrations of Fe and Ti may derive from the bones of animals, but may also be linked with higher contents of ilmenite mineral observed in layers A-D by the immersion method.

The contents of Cu, Zn and Mo are abundant in layers E, F and G; however, they are not related to human activity such as metallurgy, because the age of the layers (>41,700 BP) places them long before the Copper and Bronze Ages. An interesting result from the trace element analyses of the chert sample and layer F was obtained. X-ray study of the chert sample showed similarities with soil layer F for several elements (Cr, V, Rb, Co, Fe, Mn) (Fig. 13, A). The only chert piece, probably a tool (Fig. 13, B) was found in rubbish of washed material (unfortunately of unknown exact stratigraphic position). The aforementioned data shows the high probability of using the chert as a raw material, but more finds will be needed for future investigations.

CONCLUSIONS

- The Karin Tak cave has important tectonic control. The NW-SE trending oblique-slip faults and dominant fissures favored the cave initiation and its general orientation. The hypogenic influence in the initial stages is not

bers allowed us to map and also distinguish relatively soft deposits from harder limestone blocks resulting from the roof collapse. The excavations are focused on the central area (outlined by the dashed line in Fig. 7), which is promising in terms of archaeological and biological remains. Pollen grains were observed in layers A and B (Fig. 11) formed between 24.803–34.486 Cal BP (Antonosyan et al., 2019). The overall pollen profile is dominated by trees that are adapted to relatively moist and cool temperate areas with cool summers to very heavy winter snowfalls and ice storms. The pollen record is over-represented in conifers (>60%), which belong to the genera of *Tsuga* sp. (Fig. 11, c) and *Pinus* sp. Deciduous trees from the genres of *Fraxinus* sp. (Fig. 11, d) and *Quercus* sp., which demand comparably dry soil and are more photophilic, are relatively well-represented. These trees are more distributed in the tropical and subtropical regions of the northern hemisphere. The presence of inertinite in the cave sediment samples (equidimensional opaque in the sections) indicates a relatively long transportation distance.

The new pollen data presented in this study is consistent with the results of Antonosyan et al. (2019) and provides no evidence of dramatic climate change during LGM MIS 2.

excluded, but the presence of numerous vertical shafts in the cave together with sinkholes and speleothems indicate its principal epigenic nature.

- The geophysical, morphological, and sedimentary study indicates two major collapses of different magnitudes of presumed seismic origin. The material of the second, less pronounced collapse, forms a wedge-shaped cone, which becomes thicker below the collapsed sinkhole. The first more important collapse is the result of the roof collapse (breakdown).
- The pollen record evidence of non-dramatic climate change during LGM MIS 2 in the area and it could serve as a refugial zone for hominin activity.
- Layer F, rich in organic matter and its similarity in several elements to the chert sample (possible raw material) from the surrounding rocks, indicates hominin activity. Nevertheless, the high contents of Cu, Zn and Mo are not related to human activity such as metallurgy.

ACKNOWLEDGMENTS

This work is supported by the Science Committee of the Republic of Armenia, in the frames of the research project № 18T-1E131. The authors are grateful for constructive remarks of the anonymous reviewers that helped to significantly improve the first version of the manuscript.

REFERENCES

- Adler, D.S., Wilkinson, K.N., Blockley, S., Mark, D.F., Pinhasi, R., Schmidt-Magee, B.A., Nahapetyan, S., Mallol, C., Berna, F., Glauberman, P.J., Raczynski-Henk, Y., Wales, N., Frahm, E., Jöris, O., MacLeod, A., Smith, V.C., Cullen, V.L., and Gasparian, B., 2014 Early Levallais technology and the Lower to Middle Paleolithic transition in the Southern Caucasus: *Science*, v. 345, p. 1609–1613, <https://doi.org/10.1126/science.1256484>.
- Antonosyan, M., Seersholm, F. V., Greal, A. C., Barham, M., Werndly, D., Margaryan, A., and Yepiskoposyan, L., 2019, Ancient DNA shows high faunal diversity in the Lesser Caucasus during the Late Pleistocene: *Quaternary Science Reviews*, v. 219, p. 102–111. <https://doi.org/10.1016/j.quascirev.2019.07.012>.
- Avagyan, A., Sosson, M., Karakhanian, A., Philip, H., Rolland, Y., Melkonyan, R., and Davtyan, Y., 2010, Recent stress-field evolution in the Lesser Caucasus and adjacent regions. *in* Sosson, N., Kaymakci, N., Stephenson, R., Bergerat, F., and Starostenko, V., eds., *Sedimentary Basin Tectonics from the Black Sea and Caucasus to the Arabian Platform*, Geological Society of London, Special Publication, v. 340, p. 393–408, <http://dx.doi.org/10.1144/SP340.17>.
- Avagyan, A., Sosson, M., Sahakyan, L., Sheremet, Y., Vardanyan, S., Martirosyan, M., and Muller, C., 2018, Tectonic evolution of the South-Eastern margin of the Ararat basin, (Lesser Caucasus, Armenia): *Journal of Petroleum Geology*, v. 41, n.4, p. 495–511, <https://doi.org/10.1111/jpg.12718>.
- Bar-Yosef, O., Belfer-Cohen, A., Mesheviliani, T., Jakeli, N., Bar-Oz, G., Boaretto, E., Goldberg, P., Kvavadze, E., and Matskevich, Z., 2011. Dzuazuana: an upper palaeolithic cave site in the Caucasus foothills (Georgia): *Antiquity*, v. 85, p. 331–349. <https://www.antiquity.ac.uk/ant/085/ant0850331.htm>.
- Basta, N.T., Ryan, J.A., and Chaney, R.L., 2005, Trace element chemistry in residual treated soil: *Journal of Environment Quality*, v. 34, p. 49–63, <https://doi.org/10.2134/jeq2005.0049dup>.
- Bertacchi, A., Gasparian, G., Gruwier, B., Rivals, F., and Kandel, W.A., 2020, Upper Paleolithic animal exploitation in the Armenian Highlands: The zooarchaeology of Aghitu-3 Cave: *Quaternary International*, v. 587–588, p. 400–414. <https://doi.org/10.1016/j.quaint.2020.04.029>.
- Calvert, S.E., and Pedersen, T.F., 2007, Elemental proxies for palaeoclimatic and palaeoceanographic variability in marine sediments: interpretation and application: *in* Hillaire-Marcel, C., De Vernal, A. eds., *Proxies in Late Cenozoic Paleoclimatology: Developments in Marine Geology*, Elsevier, p. 567–644. [https://doi.org/10.1016/S1572-5480\(07\)01019-6](https://doi.org/10.1016/S1572-5480(07)01019-6).
- Clark, P.U., Dyke, A.S., Shakun, J.D., Carlson, A.E., Clark, J., Wohlfarth, B., Mitrovica, J.X., Hostetler, S.W., and McCabe, A.M., 2009, The last glacial maximum: *Science*, v. 325, p. 710–714, doi:10.1126/science.1172873.
- Domínguez-Alonso, P., Aracil, E., Porres, J.A., Andrews, P., Lynch, E.P., and Murray, J., 2016, Geology and geomorphology of Azokh Caves: *in* Azokh Cave and the Transcaucasian Corridor, Fernández-Jalvo, Y., ed., Springer, p. 55–84. DOI: 10.1007/978-3-319-24924-7_3
- Fernández-Jalvo, Y., Andrews, P., King, T., and Yepiskoposyan, L., 2016, Introduction: Azokh Cave and the Transcaucasian Corridor: *in* Delson, E., Sargis, E., eds., *Vertebrate Paleobiology and Paleoanthropology*. Springer, Dordrecht, p. 1–26, https://doi.org/10.1007/978-3-319-24924-7_1.
- Gabrielyan, A., Sarkisyan, H., Simonyan, G. 1981, *Seismotectonics of the Armenian SSR*: Yerevan State University; Pub. Yerevan, Armenian Soviet Socialist Republic, 283 p. (in Russian).
- Gabunia, L., Vekua, A., Lordkipanidze, D., 2000, The environmental contexts of early human occupation of Georgia (Transcaucasia): *Journal of Human Evolution*, v. 38, p. 785–802. <https://doi.org/10.1006/jhev.1999.0383>.
- Grichuk, V.P., Zaklinskaya, E.D., 1948, *Analiz-iskopaemykh pylyci i spor i ego primenenie v paleogeografii: (Fossil pollen and spore analysis and its application in paleogeography)*. Pub. OGIZ, Moscow, 223 p.
- Johnson, C.C., Demetriades, A., Locutura, J., and Ottesen, R.T. Eds., 2011, *Mapping the Chemical Environment of Urban Area*, First edition, Wiley-Blackwell, 640 p., <https://doi.org/10.1002/9780470670071>.
- Margaryan, A., Derenko, M., Hovhannisyants, H., Malyarchuk, B., Heller, R., Yepiskoposyan, L., Willerslev, E., and Allentoft, M. E., 2017, Eight millennia of matrilineal genetic continuity in the South Caucasus: *Current Biology*, v. 27, p. 2023–2028. <https://doi.org/10.1016/j.cub.2017.05.087>.
- Provan, J., and Bennett, K.D., 2008, Phylogeographic insights into cryptic glacial refugia: *Trends in Ecology and Evolution*, v. 23, p. 564e571. <https://doi.org/10.1016/j.tree.2008.06.010>.
- Rothwell, R.G., and Croudace, I.W., 2015, Micro-XRF studies of sediment cores: A perspective on capability and application in the environmental sciences, *in* Croudace, I. W. and Rothwell, R. G. eds., *Twenty years of XRF core scanning marine sediments: What do geochemical proxies tell us? (Developments in Paleoenvironmental Research, 17)* Dordrecht, NL: Springer, p. 25–102. https://doi.org/10.1007/978-94-017-9849-5_2.
- Shikhaylibeli, E., Abdulaev, R., Gasanov, T., Musaev, A., Panakhov, A., Gamzaev, O., and Akhundov, A., 1994. *Geologia i poleznie iskopaemie Nagornogo Karabakha*: ANA, Academie of Sciences of Azerbaijan. Institute of geology named after Academician I.M. Gubkina, p. 284 (In Russian) [Translation: Geology and minerals of Nagorno-Karabakh.]

Ara, Lilit H., Hayk, Mikayel, Kristina, Maria, Gevorg, Lilit V., Tatul, Taron, Narek, Seda, and Levon

- Sosson, M., Rolland, Y., Muller, C., Danelian, T., Melkonyan, R., Adamia, S., Kangarli, T., Avagyan, A., Galoyan, G., and Mosar, J., 2010, Subductions, obduction and collision in the Lesser Caucasus (Armenia, Azerbaijan, Georgia), new insights: *in* Sosson, M., Kaymakci, N., Stephenson, R., Bergerat, F., and Starostenko, V. eds., *Sedimentary Basin Tectonics from the Black Sea and Caucasus to the Arabian Platform: Special Volume Geological Society of London*, v. 340, p. 329–352. <http://dx.doi.org/10.1144/SP340.14>
- Stafford, T., and Yepiskoposyan, L., 2015, Cave survey, Summary of Radiocarbon, Geological and Zooarchaeological Data from Test Excavations at Karin Tak Cave, Artsakh Republic (unpublished report).
- White, W.B., 2007. Cave sediments and paleoclimate. *Journal of Cave and Karst Studies*, v. 69, p. 76–93.